Lipid biomarker-based sea surface temperature record offshore Tasmania over the last 23 million years

Suning Hou[1], Foteini Lamprou[1], Frida S. Hoem[1], Mohammad Rizky Nanda Hadju[1], Francesca Sangiorgi[1], Francien Peterse[1], Peter K. Bijl[1]

[1]Department of Earth Sciences, Utrecht University, Utrecht, 3584CB, the Netherlands

Correspondence to: Suning Hou (s.hou@uu.nl)

Abstract:

The Neogene (23.04–2.58 Ma) is characterized by progressive buildup of Antarctic and Northern Hemisphere ice volume and climate cooling. Heat/moisture delivery to Antarctica is to a large extent regulated by the strength of meridional temperature gradients. However, the evolution of the Southern Ocean frontal systems remains scarcely studied in the Neogene. Here we present the first long-term continuous sea surface temperature (SST) record of the subtropical front area in the Southern Ocean at Ocean Drilling Program (ODP) Site 1168 off western Tasmania. This site is at present located near the subtropical front (STF), as it was during the Neogene, despite a 10 degree northward tectonic drift of Tasmania. We analyzed glycerol dialkyl glycerol tetraethers (GDGTs, on 433 samples) and alkenones (on 163 samples) and reconstructed the paleotemperature evolution using TEX_{86} and $U^{k'}_{37}$ as two independent quantitative proxies. Both proxies indicate that Site 1168 experienced a temperate ~25°C during early Miocene (23–17 Ma), reaching ~29 °C during the mid-Miocene Climatic Optimum. The stepwise ~10°C cooling (20–10°C) in the mid-to-late Miocene (12.5–5.0 Ma) is larger than observed in records from lower and higher latitudes. From the Pliocene to modern (5.3–0 Ma), STF SST first plateaus at ~15°C (3 Ma), then decreases to ~6°C (1.3 Ma), and eventually increases to the modern levels around ~16 °C (0 Ma), with a higher variability of 5 degrees compared to the Miocene. Our results imply that the latitudinal temperature gradient between the Pacific equator and STF during late Miocene cooling increased from 4°C to 14°C. Meanwhile, the SST gradient between the STF and the Antarctic margin decreased due to amplified STF cooling compared to the Antarctic Margin. This implies a narrowing SST gradient in the Neogene, with contraction of warm SSTs and northward expansion of subpolar conditions.

删除了： **(sub)**

删除了： (sub)

删除了： ~~during the Neogene~~

1. Introduction

Sea surface temperature (SST) reconstructions (Rousselle et al., 2013; Zhang et al., 2014; Herbert et al., 2016; Sangiorgi et al., 2018; Super et al., 2018, 2020; Tanner et al., 2020; Van der Weijst et al., 2022) and benthic foraminiferal oxygen isotopes (Lewis et al., 2007; Holbourn et al., 2013; Lear et al., 2015; Westerhold et al., 2020; Leutert et al., 2021) demonstrated that Neogene climate cooling occurred stepwise, with episodes of intermittent warming, e.g., during the mid-Miocene climatic optimum (MCO, 16.9–15 Ma) and mid-Pliocene warm period (mPWP, 3.264–3.025 Ma). This cooling trend is further accompanied by Antarctic ice volume increase (Lewis et al., 2007; Lear et al., 2015; Leutert et al., 2021), pCO_2 decline (Sosdian et al., 2018; Super et al., 2018; Tanner et al., 2020; Rae et al., 2021), strengthening of the Antarctic Circumpolar Current (ACC, Sijp et al., 2014; Evangelinos et al., 2021) and sea ice expansion (McKay et al., 2012; Bijl et al., 2018; Sangiorgi et al., 2018), e.g., during the mid-Miocene climatic transition (MMCT, 14.5-12.5 Ma). The Southern Ocean is of special importance in reconstructions of past climate, as it plays a crucial role in ocean circulation, ocean-atmosphere carbon exchange, and as modulator of heat transport towards the largest body of land ice on Earth, the Antarctic ice sheet (Rintoul et al., 2018). The latitudinal position and strength of the ACC and its associated ocean fronts are forced by position shifts of the westerlies and bathymetry and have been suggested to modulate ocean-atmosphere CO_2 exchange as a feedback to the climate system (Toggweiler et al., 2006; Skinner et al., 2010). The gradual widening of Tasmanian gateway and Drake Passage in the Neogene provided the geographic boundary conditions for a further strengthening of the ACC and associated oceanic fronts (Sijp et al., 2014; Evangelinos et al., 2021). Yet, the evolution of the ACC in the Neogene is poorly documented, as its strength and position are difficult to constrain from geological archives. One of the manifestations of a strengthening ACC and frontal systems would be an increase in the meridional temperature gradient in the Southern Ocean, and the gradient between the Antarctic Margin and the subtropical front (STF) in particular. The latter represents the northern limit of the Southern Ocean, the northern branch of the ACC, and the boundary between the subtropical gyre and the subpolar waters, representing an oceanographic midpoint between the equator and Antarctica. While individual SST reconstructions for the Neogene Southern Ocean exist (e.g., Herbert et al., 2016), the evolution of the latitudinal SST gradient has thus far not been evaluated. Although a compilation of Antarctic ice-proximal SSTs has recently become available (Duncan et al., 2022), SST reconstructions from the more northern parts of the Southern Ocean only cover short time intervals, which precludes an integrated overview of the evolution of the latitudinal SST gradient.

We here provide a detailed reconstruction of the Neogene SST evolution of the subtropical front based on lipid biomarkers stored in sediments retrieved from Ocean Drilling Program (ODP) Site 1168, offshore western Tasmania. We base our

删除了：(sub)

删除了：MMCT

reconstruction on two independent SST proxies. The TEX_{86} paleothermometer is based on the relative number of cyclopentane moieties in isoprenoid glycerol dialkyl glycerol tetraethers (isoGDGTs) produced by marine archaea, which varies as a function of ambient temperature in a global set of marine surface sediments (Schouten et al., 2002). The $U^{k'}_{37}$ index is based on the relative abundance of di- and tri-unsaturated C_{37} alkenones synthesized by unicellular haptophyte marine algae which yield a robust relationship with SST (Volkman et al., 1980; Eglinton & Eglinton, 2008). We put our new record into context of those from regions further north and closer to Antarctica for an integrated reconstruction of Southern Ocean latitudinal SST gradients.

2. Material and methods

2.1 ODP Site 1168

Site 1168 (42°36.5809′S; 144°24.7620′E; 2463 m modern water depth) (Fig. 1) is located on the continental slope of the west-Tasmanian continental margin. The site sits on the north edge of the Subtropical Convergence zone, which separates warm, saline subtropical waters from comparably cold and fresh subantarctic water masses (Heath et al., 1985; Exon et al., 2001) with a modern SST ranging from 13-17°C (winter-summer). During the Neogene, the location of Site 1168 tectonically drifted along with Tasmania and Australia from 52°S at 23 Ma to its modern position at 42°S (Van Hinsbergen et al., 2015). During this northward tectonic drift, the Southern margin of Australia was continuously bathed by the eastward flowing proto-Leeuwin Current (McGowran et al., 2004; Hoem et al., 2021). Hence, Site 1168 is well-suited to study the Neogene evolution of the ACC and the STF.

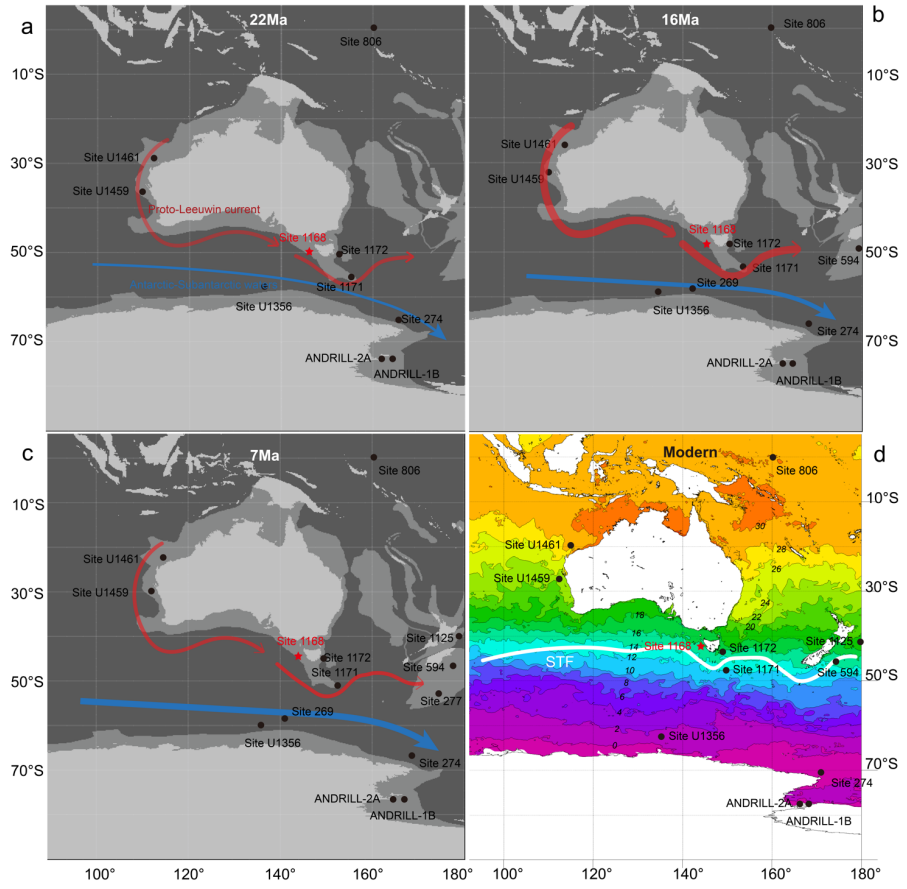

Figure 1: Neogene Paleogeographic maps of the Australian-Antarctic sector, with Deep Sea Drilling Program, the Ocean Drilling Program and Integrated Ocean Drilling Program site locations referred in this study. a, b, c: Reconstructed map of studied area using GPlates (Torsvik et al., 2012; Van Hinsbergen et al., 2015) with inferred surface ocean currents (red and blue solid lines, De Vleeschouwer et al., 2019; Jackson et al., 2019; Sauermilch et al., 2021; Evagelinos et al., 2021). The thickness of the lines denotes

the relative strength of the currents. **The edge of the light grey fill denotes present-day shorelines. The dark-grey contours indicate the edge of continental plates. Compiled sites and the site of this study are shown with black circles and red star respectively. d: Modern map (modified from NOAA) of studied area filled with modern sea surface temperature, which is indicated by colours and contours and numbers on the contours. The white line indicates the subtropical front.**

2.2 Age model

The post-cruise bio-magnetostratigraphic age model includes nannofossil, planktonic foraminifer, diatom, radiolarian, and dinocyst biostratigraphy with constraints from magnetostratigraphy and stable isotope data (Stickley et al. 2004). Here we recalibrated these datums to the Geological Time Scale 2020 (Gradstein et al., 2020), by using state-of-the-art biostratigraphic constraints from nannotax and foramtax, and updated diatom biostratigraphic constraints (Cody et al., 2008). We then fitted a loess smooth curve through these datums whereby we assign a 10-fold weight on magnetostratigraphic and benthic $\delta^{18}O$ tie points. We interpolated this loess curve to obtain ages for the samples. We derive average sediment accumulation rates of 1.8 cm/kyr for the top 360 meters (22–0 Ma) and 7.1 cm/kyr between 360 and 462 meters below sea floor (mbsf; 23–22 Ma; Fig.2).

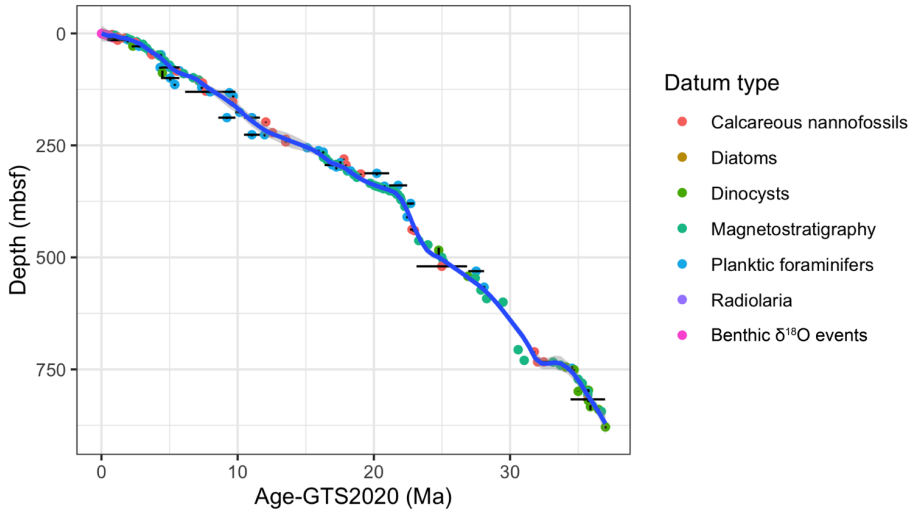

Figure 2: Age model of Site 1168. Points indicate the datums (Stickley et al., 2004). Colors indicate datum types. Blue curve indicates

the loess smooth curve with a span of 0.1 throughout the studied interval, which we resampled to obtain ages for the samples used in this study.

2.3 Lithology

A total of 883.5 meters of sediment was recovered from Site1168 Hole A, dating back to the Late Eocene to modern (Exon et al., 2001). The Neogene interval is represented in the upper 413 meters. Between 260–413 mbsf (early to mid- Miocene; 23.0–15.6 Ma), sediments comprise of clay-bearing nannofossil chalk with a gradual decrease of non-carbonate minerals (Robert, 2004). The upper 260 meters (mid-Miocene to modern; 15.6–0 Ma) contain calcareous biogenic oozes, with 85–97 wt% calcium carbonate (Exon et al., 2001), a sharp decrease in detrital clay content occurs at the boundary between these lithologic units (Robert, 2004).

2.4 Biomarker extraction and analysis

Lipid biomarkers were extracted from 433 powdered and freeze-dried samples with a Milestone Ethos X microwave system using dichloromethane: methanol (DCM:MeOH) 9:1 (v/v). Activated Al_2O_3 columns were used for the separation of the total lipid extract into 3 fractions, using solvent mixtures hexane: DCM 9:1 (v/v), hexane: DCM 1:1 (v/v) and DCM: MeOH 1:1 (v/v) for apolar, ketone and polar fractions, respectively. Polar fractions were filtered using a 0.45 µm polytetrafluorethylene filter and analysed using an Agilent 1260 Infinity series HPLC system coupled to an Agilent 6130 single quadrupole mass spectrometer, following instrumental and analytical setup as described in (Hopmans et al., 2016). 99ng of C_{46} standard was added to the polar fraction in order to quantify the absolute concentration of GDGTs. The ketone fractions of 163 out of 433 samples were dissolved in ethyl acetate and analysed on a Gas Chromatograph (GC) coupled to a flame ionisation detector (GC-FID, Hewlett Packard 6890 series) equipped with a CP-Sil 5 fused silica capillary column (25 m x 0.32 mm; film thickness 0.12 um) and a 0.53 mm precolumn. Samples were injected on-column at 70°C with helium as a carrier gas at a constant pressure of 100 kPa. The oven program was as follows: 70°C for 1 min, then ramped to 130°C at 20°C /min, then to 320°C at 4°C/min, and then held isothermal for 10 mins. Di- and tri-unsaturated C_{37} alkenones were identified based on retention time. Data is stored at Zenodo (Bijl et al., 2022).

2.5 SST reconstruction and confounding factor indices

We follow the approach by Sluijs et al. (2020) and Bijl et al. (2021) to assess non-temperature factors on the relative distribution of isoGDGTs, and thus the TEX_{86} value they represent. Briefly, this involves checking the weighted average of cyclopentane moieties of isoGDGTs compared to modern values (with the Ring Index; Zhang et al., 2016), overprints from methanotrophic archaea (with the Methane Index; Zhang et al. 2011, Weijers et al., 2011), methanogens (with the GDGT-0/Cren ratio; Blaga et al., 2009), as well as contributions from deep-dwelling archaea (with the GDGT-2/GDGT-3 ratio; Taylor et al., 2013) or terrestrial GDGTs (with the BIT index; Hopmans et al., 2004; Weijers et al., 2006). The BIT index is determined by the ratio of branched GDGTs (brGDGTs) produced by terrestrial bacteria and marine originated crenarchaeol. However, recent studies have proved that brGDGTs can be produced in situ in marine environments (Peterse et al., 2009; Sinninghe Damsté, 2016; Dearing Crampton-Flood et al., 2019). Thus, source(s) of brGDGTs are assessed using the weighted number of cyclopentane moieties in tetramethylated branched GDGTs ($\#rings_{tetra}$), where a value >0.7 is assumed to indicate a marine rather than a terrestrial source of these compounds (Sinninghe Damsté, 2016). In order to assess the influence of potential algae distribution on the $U^{k'}_{37}$-based SST reconstruction, we explored the ration between C_{37} and C_{38} (C_{37}/C_{38}) (Rosell-Melé. et al., 1994) and the ratio between all C37 and the ethyl C38 alkenones (C_{37}/C_{38Et}) (Zheng et al., 2019).

Numerous calibrations have been implemented to translate TEX_{86} into sea surface temperature (e.g., Schouten et al., 2002; Kim et al., 2010; Tierney and Tingley, 2014). However, improved understanding of archaea ecology questions the validity of TEX_{86} as a true proxy for the ocean mixed layer temperature. This is especially due to the variable export production zone depth (50-200m) of marine Thaumarchaeota. Fortunately, this can be revealed by the GDGT-2/GDGT-3 ratio, which suggests that many modern core top samples actually have contributions from deep-dwelling archaea (Van der Weijst et al., 2022). Thus, the ambient temperature of Thaumarchaeota, which determine the cyclisation of GDGTs, is not strictly sea surface temperature. Even though the GDGTs may to variable extent derive from around the thermocline, it was shown that that SST has a strong relationship with surface temperature (Van der Weijst et al., 2022). Subsurface calibrations (Tierney and Tingley, 2014; Kim et al., 2015; Ho and Laepple, 2016) use variable ways to integrate temperature over depth, which still induce uncertainty on their reliability. Nonetheless, even though a perfect calibration does not exist yet, TEX_{86} is still a valuable proxy that reflects the temperature of a relatively stable layer of the ocean (e.g. Kim et al., 2016; Hurley et al., 2018) and provides a robust ocean temperature change in both trend and variability (Van der Weijst et al., 2022). Because the relationship between the TEX_{86} in sediments and surface temperature actually derives from the strong relationship between subsurface and surface temperature.

删除了：，

删除了： Hopmans et al., 2004)

删除了：，

Especially, when TEX_{86} is used along with other temperature proxies (e.g. Super et al., 2020, Leutert et al., 2020), which we here use $U^{k'}_{37}$, both proxies together can provide better constrains on SST reconstructions.

Here, we apply the spatial linear Bayesian calibration BAYSPAR (Tierney and Tingley, 2014; 2015) to translate TEX_{86} values into temperatures using both surface (0–20 m) and depth-integrated temperature (0–200 m) calibrations (prior mean of 20°C, prior standard deviation of 20°C). We applied the $U^{k'}_{37}$ paleothermometer based on alkenones as independent additional paleothermometer. $U^{k'}_{37}$ index values were calculated following Prahl and Wakeham (1987) and converted to SST using the BAYSPLINE calibration of Tierney and Tingley (2018) (prior standard deviation of 10°C). We choose the Bayesian calibrations for both proxies in consideration of both high-temperature applicability and spatial characteristics. These two proxies together with the TEX_{86} related overprint indices are combined to determine the sea surface temperature (SST) change.

3. Results

3.1 GDGT-based temperature reconstruction

Our new GDGTs data is derived from 412.7 to 0 mbsf (22.6-0 Ma). The concentrations of all GDGTs are consistently high (~50 μg/g sediment for total isoGDGTs) in the early Miocene, and show a normal relative distribution, except for the interval around the MCO (287–256 mbsf). The isoGDGT concentration drops to 5 ug/g sediment at the onset of the MCO and remains stable until 7 Ma. In the MCO interval, of all GDGTs, crenarchaeol (Cren) and crenarchaeol (Cren') decreases the strongest (to 1/400, GDGT-3 decreases to 1/200, GDGT-2 and GDGT-1 decreases to 1/100, GDGT-0 decreases to 1/25; Suppl. Fig. 1). As Cren is not in the TEX_{86} index, its anomalous trends in abundance do not directly affect TEX_{86} values but do affect the GDGT indices and ratios that have Cren in the denominator. As a result of the extra decline in Cren, GDGT-0/Cren, MI and GDGT-2/Cren all yield abnormally high values in the MCO interval (Fig. 3). The GDGT-2/3 ratio is gradually increasing from 5 to 8 throughout the record, with transient peaks in the early Miocene and MCO. Cut-off values for this ratio vary among users and sites, between 3 and 10 (e.g., Leutert et al., 2020; Bijl et al., 2021; Van der Weijst et al., 2022). Hurley et al. (2018) demonstrated that the GDGT-2/GDGT-3 values rapidly rise from 3–5 in the surface mixed layer (upper 150m) to 20–25 at the thermocline depth (see also Basse et al., 2014; Hernández-Sánchez et al., 2014; Kim et al., 2016; Van der Weijst et al., 2022). In any case, sediments with GDGT-2/GDGT-3 values >3 might to some extent be biased towards deeper waters and, thus, to lower temperatures. ΔRing Index varied from -2.2 to 1 in the whole record and 152 data points fall outside the 95% confidence interval of the RI-TEX_{86} array (Suppl. Fig. 3).

BIT index values show a large range of variation, between 0.1 and 0.9, and show a prominent peak (~ 0.9) during the MCO, and consistent low values (~0.1) in the Pliocene, indicating a potentially large contribution of GDGTs from land (Fig. 3).

删除了： it

删除了： as well

设置了格式： 英语(美国)

删除了： (sub)

However, the #rings$_{tetra}$ values highly varied throughout time, but are consistently elevated between 17 and 7 Ma from 0.3 to more than 1.0, suggesting that brGDGTs have an in situ marine origin. In a ternary diagram of the tetra-, penta-, and hexa-methylated brGDGTs, Site 1168 samples plot generally offset to the global soil cluster (Suppl. Fig. 4), which also supports a non-soil origin. This would imply that the BIT index cannot be interpreted as indicator for the input of terrestrial matter at this site.

TEX_{86} values of the early Miocene were around 0.65 but fluctuating, then reached 0.8 at 16 Ma in the MCO interval, although these values are probably affected by non-thermal overprints. There is an abrupt decline in TEX_{86} values after the MCO and then a long-term decrease to 0.4 until 5 Ma. TEX_{86} values increased to 0.6 in the early Pliocene, then decreased to 0.36 at 1.35 Ma, and eventually increased to 0.52 in the youngest sediment (Fig. 3). SSTs derived from the TEX_{86} are around 25°C in the early Miocene section. TEX_{86} values at the peak MCO would equate to SSTs of 34°C, followed by first a rapid cooling at around 14.5 Ma, and then more gradual down to 7°C towards the end of the Miocene (Fig. 4). After an ephemeral warming in the early Pliocene to 20°C, SST decreased to 6°C in the mid-Pleistocene, and then recovered to the modern level around 17°C. Throughout the record, the difference in temperature derived from surface and depth-integrated sub-surface calibrations respectively is small (< 2°C).

删除了： difference between

删除了： temperature derived from TEX_{86}

3.2 Alkenone-based temperature reconstruction

Our new alkenone data is derived from 363 to 0 mbsf (21.9-0 Ma). Existing $U^{k'}_{37}$ data from this site was published in (Guitián and Stoll, 2021). C_{38} alkenones are mostly at or below detection limit in the sediments older than 8 Ma. In the younger sediments we find 4 clear peaks representing C_{38} alkenones. Here, C_{37}/C_{38} fluctuates between 0.9 and 1.2 while C_{37}/C_{38Et} varies between 1.2 and 1.4 (Suppl. Fig. 5). The $U^{k'}_{37}$ index record varies between 0.43 and 0.93, and generally follows the trends of TEX_{86}, except during the MCO and the early Pleistocene (Fig. 4). Early Miocene sediments have an average $U^{k'}_{37}$ value of ~0.8, in agreement with previously published data from the same site (Guitián and Stoll, 2021). In the MCO interval, $U^{k'}_{37}$ rose to 0.93. None of the analyzed sediments in the MCO interval have saturated $U^{k'}_{37}$ index values. Subsequently, $U^{k'}_{37}$ gradually drops to 0.43 in the end of the Miocene and recovers to ~0.6 in the Pliocene. $U^{k'}_{37}$-based SST reveal similar temperatures to TEX_{86}-based SubT except in the MCO interval (Fig. 4). In the early Miocene, SST_{UK37} yields ~24°C on average, then increases to ~28°C in the MCO. Subsequently SST_{UK37} cools down to 10°C at 5 Ma and increases to 16°C in the Pliocene. SST_{UK37} shows a similar trend as SST_{TEX} in the Pleistocene and varies between 17°C and 7.5°C. However, the difference

设置了格式： 字体颜色：自动设置

between SST_{UK37} and SST_{TEX} increases since the onset of the Pleistocene, due to the plunge of SST_{TEX}.

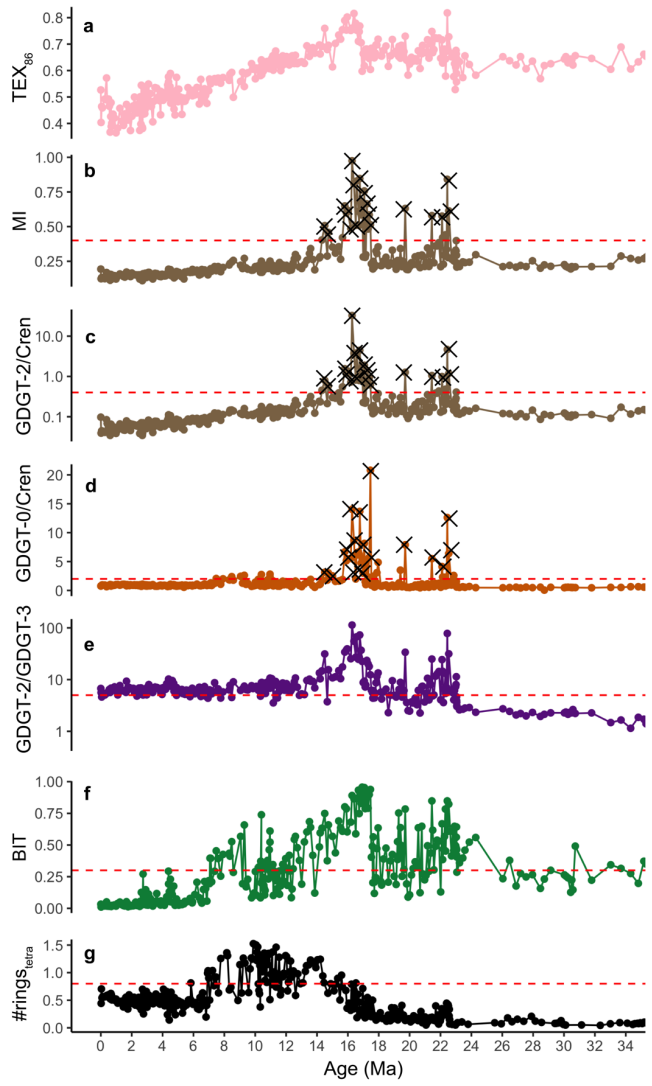
a
TEX_{86}
0.8
0.7
0.6
0.5
0.4
b
MI
1.00
0.75
0.50
0.25
c
GDGT-2/Cren
10.0
1.0
0.1
d
GDGT-0/Cren
20
15
10
5
0
e
GDGT-2/GDGT-3
100
10
1
f
BIT
1.00
0.75
0.50
0.25
0.00
g
$\#rings_{tetra}$
1.5
1.0
0.5
0.0
0 2 4 6 8 10 12 14 16 18 20 22 24 26 28 30 32 34
Age (Ma)

Figure 3. TEX_{86} values and indices/ratios to detect non-thermal GDGT contributions. Red dashed lines indicate proposed threshold values. a. TEX_{86}. b. Methane index, threshold=0.4 (Zhang et al., 2011) c. GDGT-2/Cren, threshold=0.4 (Weijers et al., 2011). d. GDGT-0/Cren, threshold=2 (Blaga et al., 2009). f. BIT, usually applied threshold=0.3 (Hopmans et al., 2004). e. GDGT-2/GDGT-3, threshold=5 (Taylor et al., 2013). g.#$rings_{tetra}$, threshold=0.8 (Sinninghe Damsté, 2016). Discarded data are shown by crosses.

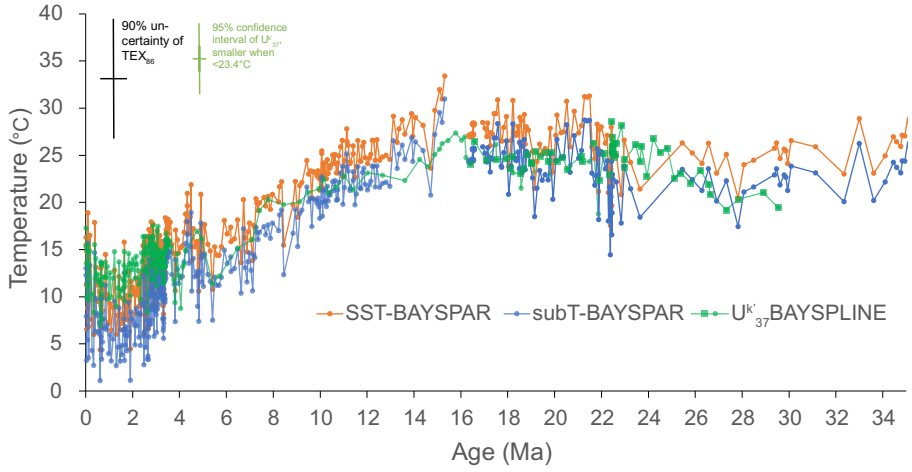

Figure 4. TEX_{86} and $U^{k'}_{37}$ SST reconstructions of Site 1168. The BAYSPAR calibration (Tierney and Tingley, 2014) is used to translate TEX_{86} values into surface (orange points) and subsurface (blue points) temperatures. $U^{k'}_{37}$ SST reconstruction (dark green) based on the BAYSPLINE calibration (Tierney and Tingley, 2018). All new data are denoted by dots. Oligocene–early Miocene $U^{k'}_{37}$ SSTs of Guitián and Stoll (2021) are represented by green squares.

删除了：；

删除了：）

4. Discussion

4.1 Reliability assessment of the SST record

In all intervals of the records besides the MCO, temperature estimates derived from the $U^{k'}_{37}$ and TEX_{86} have similar trends and absolute temperatures, demonstrating that both proxies represent the same water layer. The large $U^{k'}_{37}$/TEX_{86} discrepancy

during the MCO suggests that one of the paleotemperature proxies is affected by non-thermal overprints (Fig. 4, 5). Given the many indices that signal anomalous isoGDGT distributions in the MCO interval, it is likely TEX_{86} that has a non-pelagic GDGT assemblage and thus reflects an unreliable SST. However, the high GDGT-0/Cren, MI, GDGT-2/Cren and BIT index values in the MCO interval are all caused by the anomalously low contribution of Cren (i.e., the denominator) and not of elevated relative abundances of the signaling compound for that overprint (the nominator). Moreover, the low TOC wt% (<0.5%) (Exon et al., 2001) in the MCO sediments does not support the existence of any cold seeps, anaerobic oxidation of methane or methane hydrate production, despite the high GDGT-0/Cren, MI and GDGT-2/Cren values (Fig. 3). If it is indeed the excess relative decrease in Cren concentration that causes the high BIT, GDGT-0/Cren, MI, GDGT-2/Cren and low RI, because all have Cren involved in their equation, the question is to what extent this affects TEX_{86} values. In any case, the indices may not necessarily reflect the overprints that they are usually associated to at this site. However, since in the same interval as the anomalous GDGT compositions TEX_{86} and $U^{k'}_{37}$ disagree, and to be conservative, we discard the TEX_{86}-based SSTs with high confounding factor values in the MCO interval at this site.

The anomalously low relative abundance of Cren could be explained by different preservation efficiency and/or degradation rates for distinct GDGTs. The interval in which GDGT concentrations decrease (17.34–16.85 Ma, 294.66–274.28 mbsf) is concomitant to an interval of decreased terrigenous clay and quartz and increased calcium carbonate content (Fig. 5; Robert, 2004). The loss of terrigenous clay can lead to reduced preservation of organic matter (Ransom et al., 1998; Wu et al., 2019) because enhanced pore-water flow in the overlying sediment enhances oxygen exposure time (Huguet et al., 2008; Schouten et al., 2013). It was shown that isoGDGTs with more cyclopentane moieties are less resistant to oxidation than those with less cyclopentanes (Ding et al., 2013). As a result, degradation processes would result in lower TEX_{86} values and an underestimation of SSTs. However, in the MCO interval TEX_{86} was very high and led to SST reconstructions much higher than SST_{UK37}. While selective degradation could be an explanation for the relatively excessive loss of Cren, it cannot explain the anomalously high TEX_{86}-based SSTs in that interval. On the other hand, preferential degradation of alkenones could have biased $U^{k'}_{37}$ at this site as well, notably in the form of a warm bias in SST (Freitas et al., 2017). Yet, in the MCO interval, we do not observe anomalous warmth, and the index is not yet saturated. Therefore, the selective degradation in alkenones cannot explain the SST difference between SSTs derived from $U^{k'}_{37}$ and TEX_{86}.

The extremely high (up to 100) GDGT-2/GDGT-3 ratio found in the MCO is unprecedented in both paleo and modern ocean records (e.g., Taylor et al., 2013; Hernández-Sánchez et al., 2014; Hurley et al., 2018; Besseling et al., 2019; Bijl et al., 2021; Van der Weijst et al., 2022). Perhaps the isoGDGTs found in the MCO interval were produced by other archaeal communities, e.g., Marine Group II and/or III (Besseling et al., 2019) and the ratio could have been further increased through selective

degradation of GDGT-3 over GDGT-2. Given the temperature trend in the MCO interval, these GDGT producers may have also responded to water temperature, although indirectly or with a different dependency. In the early and late Miocene, GDGT-2/GDGT-3 values are still relatively high (>5), indicating some isoGDGT input from deep water sources. The overall input of deeper-dwelling GDGTs may bias the reconstruction of absolute SST from TEX_{86}, but because the GDGT2/3 ratio in our post MMCT interval is stable and without a trend, the trend of TEX_{86} should not be influenced (Ho and Laepple, 2016; Leutert et al., 2020; Van der Weijst et al., 2022) and the amplitude is well constrained by $U^{k'}_{37}$. Thus, for the late Miocene and Pliocene the sediments are not discarded, despite high GDGT-2/GDGT-3 values. Despite nearly half of the data points falling out of the 95% confidence interval of TEX_{86}-Ring Index, we decided to not discard those because most of the sediments with abnormal ring index values are caused by the highly reduced contribution of Cren.

C_{37}/C_{38} and C_{37}/C_{38Et} ratios do not show any profound change, thus we infer that alkenone composition is not affected by algae composition changes and thus $U^{k'}_{37}$ represents sea surface temperature. While TEX_{86}-derived SST is in a consistently in similar range or above $U^{k'}_{37}$-derived SST throughout most of the record, with the onset of the Pleistocene SST_{TEX} drops significantly when compared to those derived from alkenones. But the difference is around 3°C, which is still within the calibration errors. Nevertheless, such difference is mainly due to the use of BAYSPAR calibration. SST results using BAYSPAR calibration are barely different from TEX_{86}^{H} based on the temperature output when TEX_{86}>0.5. However, when TEX_{86} is smaller than 0.5, namely in the Pleistocene, TEX_{86}^{H}-based SST is well in line with SST_{UK37} (Suppl. Fig. 6).

Overall, considering the small difference (~2°C) between surface and subsurface calibration of TEX_{86} and SST_{UK37}, the relatively large calibration error of proxies and similar extent of variability and the high GDGT-2/GDGT-3 ratio throughout the study interval, we deem that both proxies mainly reflect temperature of the surface layer, with TEX_{86} integrating a deeper component. Hence, we claim our temperature record a sea surface temperature (SST). But we focus on the $U^{k'}_{37}$ record when we interpret the record during the MCO.

删除了： MMCT

删除了： (sub)

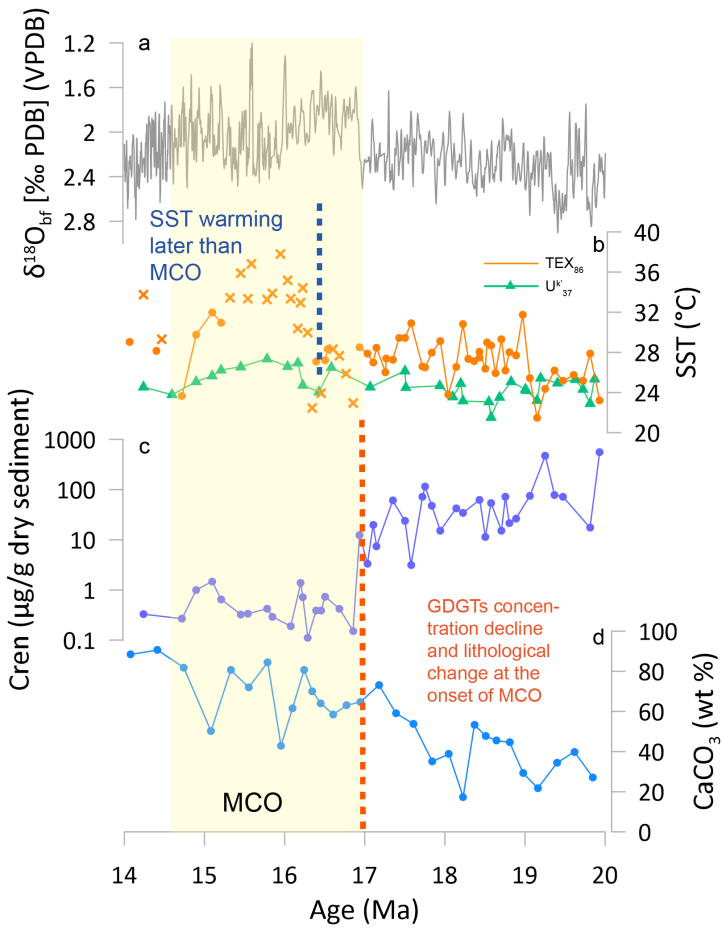

Figure 5: Lithology, GDGT concentrations and relative distributions and SST change in the mid-Miocene. a. Benthic foraminiferal $\delta^{18}O$ compilation (Westerhold et al., 2020) b. SST changes based on TEX_{86} and $U^{k'}_{37}$ (this study and Guitián and Stoll, 2020). Orange dots indicate data points that are considered reliable and crosses indicate data points of TEX_{86} that are considered unreliable c. absolute abundance of Cren as indicator of GDGT preservation. d. Weight% calcium carbonate indicating lithology change,

inversely related to clay content (Robert, 2004). Orange dashed line indicates the change of lithology, while isoGDGT preservation changes occur at the onset of MCO. Blue dash line indicates the SST warming, postdating the MCO. Yellow bar indicates the interval of MCO.

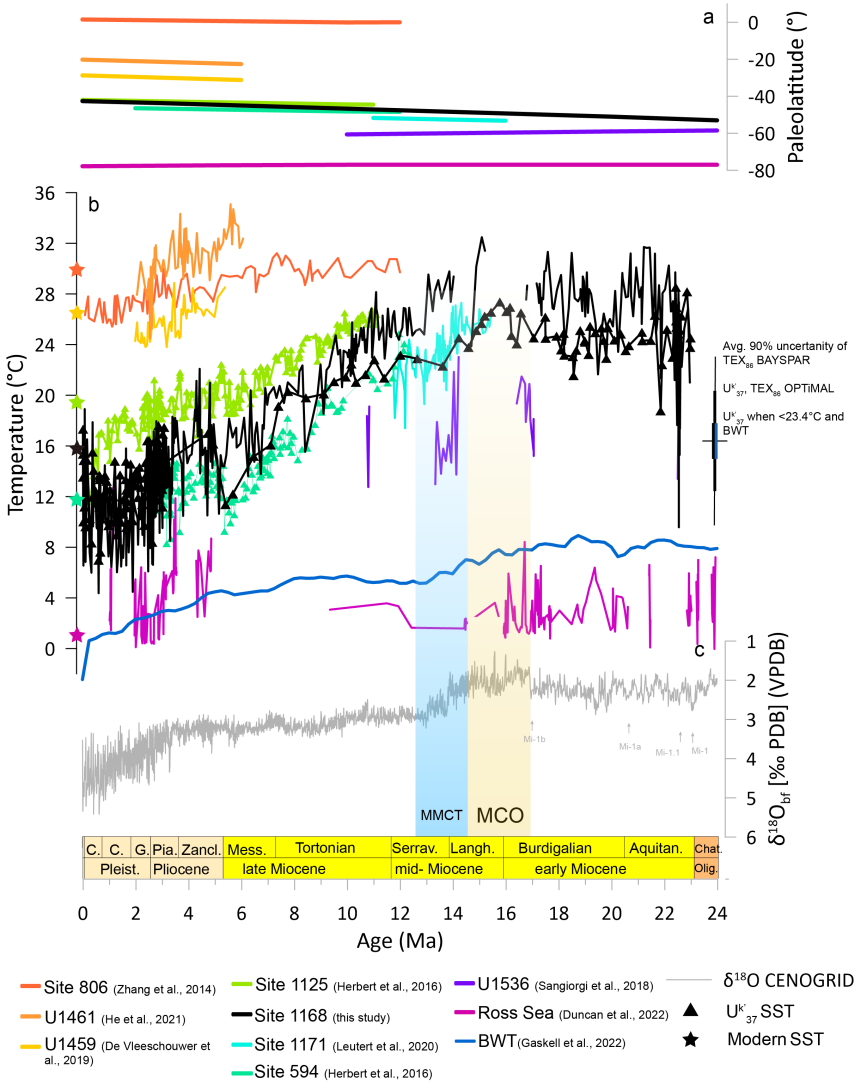
a
0
-20
-40
-60
-80
Paleolatitude (°)
b
36
32
28
24
20
16
12
8
4
0
Temperature (°C)
Avg. 90% uncertainty of TEX86 BAYSPAR
U'37, TEX86 OPTiMAL
U'37 when <23.4°C and BWT
c
1
2
3
4
5
6
δ18Obf [‰ PDB] (VPDB)
Mi-1b
Mi-1a
Mi-1.1
Mi-1
MMCT
MCO
C.
C.
G.
Pia.
Zancl.
Mess.
Tortonian
Serrav.
Langh.
Burdigalian
Aquitan.
Chat.
Pleist.
Pliocene
late Miocene
mid- Miocene
early Miocene
Olig.
0
2
4
6
8
10
12
14
16
18
20
22
24
Age (Ma)
Site 806 (Zhang et al., 2014)
U1461 (He et al., 2021)
U1459 (De Vleeschouwer et al., 2019)
Site 1125 (Herbert et al., 2016)
Site 1168 (this study)
Site 1171 (Leutert et al., 2020)
Site 594 (Herbert et al., 2016)
U1536 (Sangiorgi et al., 2018)
Ross Sea (Duncan et al., 2022)
BWT (Gaskell et al., 2022)
δ18O CENOGRID
U'37 SST
Modern SST

Figure 6: a. Paleolatitude reconstruction using GPlates (Torsvik et al., 2012; Van Hinsbergen et al., 2015) of Site 1168 (this study, Guitián and Stoll, 2021), Site 806 (Zhang et al., 2014), Site U1461 (He et al., 2021), Site 1171 (Leutert et al., 2020), Site U1459 (De Vleeschouwer et al., 2019), Site 594, Site 1125 (Herbert et al., 2016), Site U1356 (Hartman et al., 2018; Sangiorgi et al., 2018), the Ross Sea compilation (AND-1B, AND-2A, DSDP 274, DSDP 270, CIROS 1, CRP 2/2A; McKay et al., 2012; Levy et al., 2016; Sangiorgi et al., 2020; Duncan et al., 2022) b. Reconstructed SST of the same sites using BAYSPAR and OPTiMAL (Ross Sea only) calibrations for TEX_{86} (no symbol) and BAYSPLINE for $U^{k'}_{37}$ (triangles) and bottom water temperature based on benthic foraminiferal $\delta^{18}O$ (Gaskell et al., 2022). c. Benthic foraminiferal $\delta^{18}O$ compilation (Westerhold et al., 2020). Modern SSTs of the sites are indicated by the coloured stars at 0 Ma.

4.2 Site1168 SST evolution and Southern Ocean temperature gradient in the Neogene

The new SST record for Site 1168 shows in broad lines a similar trend to the global compilation of benthic foraminiferal oxygen isotope stack ($\delta^{18}O_{bf}$), however there are some interesting deviations (Fig. 6). The mid-to-late Miocene interval contains a remarkable ~10°C gradual SST cooling that is much less prominent in $\delta^{18}O_{bf}$ (Fig. 6). Other than the late Miocene cooling, we have found that subtropical SSTs fluctuated around 26°C in the early Miocene, which is similar to those in the Oligocene (Fig. 4) (Guitian and Stoll, 2021; Hoem et al., 2022). The SST record from >23 Ma is elaborately discussed in Hoem et al. (2022) so we will focus on the SST trends in the interval <23 Ma. SSTs were slightly elevated in the MCO and rapidly cooled 5°C across the MMCT. Pliocene and Pleistocene SSTs at Site 1168 have larger variability than those in the late Miocene. But the variability remains in the Pliocene and Pleistocene, which deviates from $\delta^{18}O_{bf}$ feature.

删除了： MMCT

The northward movement of the site, from ~52°S in the early Miocene to ~42°S at present, may have dampened the amplitude of Neogene long-term cooling to an unknown extent. However, during the Oligocene, ocean conditions at this site also barely changed, despite the northward drift, likely because the ocean currents migrated northwards along with the tectonic drift of Australia (Hoem et al., 2021). For the same reason, northward tectonic drift of Australia during the Neogene, in other words the latitude change, may have had similarly little effect on the temperature evolution at this site, thus records the temperature resulting in both global climate and water mass change at Site 1168. The synchronous tectonic drift of other mid-latitude sites warrants the conclusion about latitudinal temperature gradient drawn from the comparison (Fig. 6a). With the consistency of both paleotemperature proxy results in consideration, we will further discuss the SST evolution per time interval, focusing on variability within the record, comparison to the $\delta^{18}O_{bf}$ as representation of deep-sea temperature and global ice volume trends, and comparison to other SST records in the region to reconstruct latitudinal SST gradients.

Early Miocene (23.04–17.0 Ma)

In the early Miocene, SST was around 26°C, but punctuated by several short cooling events (Fig. 6). SST minima occurred at 22.4 Ma, 19.5 Ma and 17 Ma, roughly time-equivalent to ephemeral positive excursion events (Mi-1.1, Mi-1a, Mi-1b) in $\delta^{18}O_{bf}$ (Miller et al., 1991; Billups et al., 2002; Liebrand et al., 2011; Westerhold et al., 2020). SSTs from the Wilkes Land margin (U1356) reflect similar events at 22.4 Ma and 17 Ma (Sangiorgi et al., 2018; Hartman et al., 2018). In contrast, SSTs in the Ross Sea remained relatively stable and profoundly cooler than U1356, around 4°C using the OPTiMAL calibration (Duncan et al., 2022). We choose OPTiMAL as the calibration for the Ross Sea sites because the Ross Sea has experienced glacial phases in the early and middle Miocene (Passchier et al., 2011; Marschalek et al., 2021) while the Wilkes Land was continued to be surrounded by warm oligotrophic waters (Bijl et al., 2018; Sangiorgi et al., 2018).

The latitudinal SST gradient between the STF and the higher latitudes was relatively constant during the early Miocene, remaining around 9°C (Fig. 7). This gradient is very similar to the modern gradient between 51°S and Antarctic margin (10°C; Fig. 1, 7; Hartman et al., 2018), and represents a similar gradient to that of the late Oligocene (Hoem et al., 2022). Such a gradient may testify to the presence of a relatively strong proto-ACC when the Tasmanian Gateway aligned to the westerly winds (Pfuhl et al., 2004; Scher et al., 2015; Sauermilch et al., 2021), although the absolute SSTs at both sites were higher in the Miocene than today (Fig. 6).

A recent study (Kim and Zhang, 2022) suggested that a massive methane hydrate destabilization event took place at the south Australian Margin during the Oligocene-Miocene boundary based on an elevated MI and more negative compound specific carbon isotopes of Site 1168. However, based on the age model of Stickley et al. (2004) calibrated to GTS 2020, the Oligocene-Miocene boundary indicated by Kim and Zhang (2022) at ~416 mbsf is actually around 22.6 Ma. On the other hand, the high MI is actually induced by less Cren and more GDGT-0, rather than an increase in GDGT-1,2,3 (Suppl. Fig. 1) which are thought to be produced by methanotrophic archaea. Thus, we doubt if the evidence is concrete enough to prove a major methane hydrates dissociation in the early Miocene but acknowledge their hypothesis.

MCO (17.0–14.5 Ma)

SST_{UK37} shows a slight warming of ~2 degrees to ~27°C at the onset of the MCO (Fig.5, 6). As this warming cannot be ascribed to saturation of the proxy, this would mean that the SST increase during the MCO is indeed smaller at the STF than at high latitude sites, and than what would be assumed from the strong change in $\delta^{18}O_{bf}$ at this time. Still, also at Site 1168, the mid-Miocene stands out as a warm time interval, consistent with other records, both surface and bottom (Levy et al., 2016; Sangiorgi

et al., 2018; Modestou et al., 2020). Compared to the clear trends in the global $\delta^{18}O_{bf}$ record (Westerhold et al., 2020), the onset of the MCO is less clearly expressed in the records of SST (this study, Shevenell et al., 2004; Levy et al., 2016; Hartman et al., 2018; Super et al., 2018, 2020) and Mg/Ca based bottom water temperature (Lear et al., 2015). Hence, the relationships between changes in surface oceanography, ice volume, and deep-sea temperature at the MCO onset remain unresolved at this stage. In addition, the currently available clumped isotope records do not fully capture the 16–17 Ma interval (Modestou et al., 2020; Meckler et al., 2022) which makes disentangling ice volume and deep-sea temperature effects in $\delta^{18}O_{bf}$ at the MCO onset problematic.

The lithological change of Site 1168 at the onset of the MCO coincides with the biomarker preservation change, but precedes regional warming and $\delta^{18}O_{bf}$ decline (Fig. 5). The increase of calcium carbonate indicates a change in the depositional setting, likely due to an intensification of the Proto-Leeuwin Current (PLC). The intensification of the PLC during MCO is interpreted from deepest seabed scouring (Jackson et al., 2019). The reported existence of 'larger foraminifera' (Gouley and Gallagher, 2004) and, perhaps, although debated, tropical corals (McGowran et al., 1997) in the Great Australian Bight (Fig. 1) are likely related to the warm water induced by PLC. Besides the increase of surface calcite productivity, this led to better ventilated bottom water and warm oligotrophic surface water conditions during MCO. The potentially limited preservation of GDGTs may be related to improved bottom water oxygenation (Huguet et al., 2008).

The SST records from Site1168, near the subtropical front, and Site 1171, in the subantarctic zone, suggest that the latitudinal SST gradient collapsed to 0 (Fig. 7). This implies that the latitudinal SST gradient across the Tasmanian Gateway was strongly reduced in the MCO. The reduced latitudinal temperature gradient persisted both equatorward and poleward. Similarly, in the eastern Equatorial Pacific (Rousselle et al., 2013), the latitudinal SST difference between the equator and subtropical region was reduced to ~2°C. We also note that the SSTs of Site 1168 and high latitude sites (Wilkes land, Ross Sea) are close to each other (Fig. 7), even though SST reconstructions of high latitude sites are sparse (U1356) and absolute values are highly dependent on the used calibration (Ross Sea sites) (Fig. 6). The reduced latitudinal SST gradient between mid-latitude and polar region (Fig. 6, 7) agrees with certain modeled results for the MCO (Herold et al., 2011; 2012) but is not captured by other modeling (Burls et al., 2021). The weakened latitudinal SST gradient means that the ACC and associated fronts were weaker and/or located closer to Antarctica. Meanwhile, enhanced evaporation led to more precipitation in the high latitudes, at least on the Antarctic continental margin (Sangiorgi et al., 2018). The global heat transport also likely weakened with latitudinally more equable latitudinal climates (Chiang, 2009).

设置了格式： 字体颜色：自动设置

删除了： as well as the existence of tropical corals (McGowran et al., 1997) and 'larger foraminifera' (Gouley and Gallagher, 2004) in the Great Australian Bight (Fig. 1)

设置了格式： 字体颜色：自动设置

删除了： The weakened latitudinal SST gradient means that the proto-ACC was reduced in strength (Sangiorgi et al., 2018) compared to during the early Miocene.

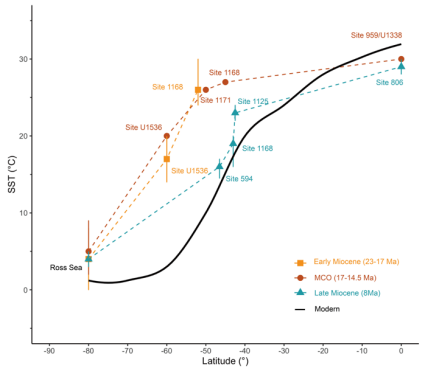

Figure 7: Sea surface latitudinal temperature gradient in the southern hemisphere, of the early Miocene (orange; 23-17 Ma), MCO (red; 17-14.5 Ma), late Miocene (blue; 8 Ma) and modern at 160°E (black; based on Fig. 1d), respectively. Error bars indicate the variability of the time range. Paleo data are from the sources in Figure 6 except for the MCO SST at equator, which are from Rouselle et al. (2013), Van der Weijst et al. (2022).

删除了：**(sub)**

MMCT (14.5–12.5 Ma)

删除了：**MMCT**

The termination of the MCO is reflected by a sharp 5°C decrease in SST at Site 1168 from 14.5 to 13 Ma, coincident with the time of cooling at nearby Site 1171 (Leutert et al., 2020) (Fig. 6). This cooling phase coincided with a strong increase in $\delta^{18}O_{bf}$, which mostly reflects Antarctic ice sheet expansion (Shevenell et al., 2004, 2008; Leutert et al., 2020) and potential northward expansion of subantarctic waters (Leutert et al., 2020) accompanied by pCO_2 decline (Super et al., 2018). The SST gradient between the mid- (Site 1168 and Site 1171) and high latitudes (Site U1356) increased, suggesting stronger fronts with amplified cooling towards Antarctica (Fig. 6). This is most likely a result of polar amplification of cooling towards high latitudes, further exacerbated by the expanding ice sheet and northward migration of frontal systems.

Late Miocene (12.5–5.3 Ma)

After the MMCT, SSTs at Site 1168 gradually cooled by 10 °C from 13 to 5 Ma and the short-term variability amplitude was notably small (2–3°C) (Fig. 6). The amplitude of this cooling is comparable to that at other mid-latitude sites, i.e., Site 594 and Site 1125 in the southwest Pacific (Herbert et al., 2016).

删除了：MMCT

The absolute temperatures and the cooling trend in the SST record of Site 594 seem in agreement with those at Site 1171, which is located at the same latitude and bathed by the same subantarctic water in the modern system. Thus, we can consider Site 1171 and Site 594 as one continuous record representing the ocean temperature 5° south to Site 1168. Furthermore, the temperature difference between closely located subtropical (Site 1125, Site 1168) and subantarctic (Site 594, Site 1171) sites became larger, about 4°C between each area (Fig. 6, 7). We deduce from this that the STF progressively got stronger. The equator-mid latitude temperature gradient also progressively increased (Fig. 7). Equatorial SST of Site 806 in the west Pacific decreased only 3°C from 12 Ma to 5 Ma (Zhang et al., 2014). Given the low temperatures at the high latitudes by the end of the Miocene (Gaskell et al., 2022) (Fig. 6), the Southern Ocean equator-to-pole latitudinal temperature gradient and the SSTs of the studied sites must have been very similar (~26°C) to modern conditions. Notably, the relatively strong Southern Ocean cooling trend is not reflected in the $\delta^{18}O_{bf}$ record, which remained relatively stable over this time interval. Thus, the relationship between Southern Ocean cooling, deep sea temperature change, and ice volume change still needs further study for this interval. The increased SST gradient reflects a combination of global cooling and the amplification effect of northward migration of the STF, which effectively stretches the Southern Ocean over wider latitudes. This change in temperature gradient between equatorial sites and Site 1168 also indicates a weakening of the Leeuwin current (De Vleeschouwer et al., 2019). The gradually increased equator to mid-high latitude SST gradient led to a contracted and strengthened Hadley cell, which consequently caused an aridification in subtropical region by intensifying the evaporation in the descending limb (Herbert et al., 2016; Groeneveld et al., 2017). This is reflected at Site 1168 and other Tasmanian sites with an increase in the contribution of kaolinite and/or illite, reflecting erosion of old soils as a result of aridification of the hinterland and subsequent transport by the westerlies since the late Miocene (since ~200 mbsf of Site 1168; Robert, 2004).

During 8–5.3 Ma, several stepwise changes occur in the Southern Ocean. Tanner et al. (2020) indicated a northward STF shift at the Agulhas ridge from 8 Ma onwards, while Groeneveld et al. (2017) suggested a southward migration of the westerlies near southwest Australia in the same period. This apparent discrepancy can be partly accounted for with the northward tectonic movement of Australia while the STF remained at its position, or moved northward at a slower pace than the continent (De Vleeschouwer et al., 2019), while the Agulhas plateau experienced limited tectonic movement. This would mean that Site 1168 entered the subtropical zone, received more warm subtropical water through Leeuwin current, and therefore would reduce the temperature difference between west Australian coastal sites. However, the increased SST difference that we observe between Site 1168 and northwest Australia/equator (Fig. 6) suggest a weaker PLC, and thus does not seem to support this interpretation. Another explanation of the discrepancy between Tanner et al. (2020) and Groeneveld et al. (2017) is that the STF did not

necessarily align to the position of the westerlies (De Boer et al., 2013). The relative positional shift between the Australian continent and the westerlies does not directly influence the position of the STF when the STF remains bound by the southern edge of the Australian continent during this time. Christensen et al. (2021) suggests that changes in the Tasman leakage around 7 Ma may have an influence on the global circulation, in accordance with a southward migration of the westerlies. However, the Tasman leakage represents an intermediate water layer (400-900 m) which would not necessarily have influenced SST. Indeed, the SST record does not show a prominent, step-wise change around the time of the onset of Tasman Leakage.

Pliocene to modern (5.3–0 Ma)

Following late Miocene cooling from its minimum in the latest Miocene (Herbert et al., 2016), the Pliocene SSTs of Site 1168 shifted back to generally warm conditions (16 °C) (Fig. 6). Compared to the modest variability in $\delta^{18}O_{bf}$ in the Pliocene, SST change at the STF is relatively large in amplitude (8°C). The early Pliocene warmth found at site 1168 coincides with the SST record of the northwest Australian continental shelf (He et al., 2021), thus confirming the existence of a relatively strong Leeuwin current which causes the SST rise. The subsequent cooling after 4 Ma until the mid-Pleistocene led to an increased SST gradient between Site 1168 and west Australian coast sites along the Leeuwin current pathway, therefore, indicating a stepwise weakening (De Vleeschouer et al., 2019) (Fig. 6). The Pliocene SST variability at Site 1168 may be amplified by the combined effects of a changing Leeuwin current, migrating STF, and strong ice sheet fluctuation on Antarctica, and the variability would then be stronger than during the Miocene. SST shifts can be roughly correlated to known $\delta^{18}O_{bf}$ events, such as mid Piacenzian Warm Period and M2 glaciation. Intriguingly, in the Pliocene-Pleistocene interval, the SST of Site 1168 varied synchronously with that in the Ross Sea, which lead to a constant temperature gradient of ~8°C between mid- and high latitudes.

删除了： based on the TEX_{86}

In summary, the Neogene SST record of the STF is characterized by 5 phases of accelerated cooling of ~2–3 degrees cooling at ~14 Ma, 9 Ma, 7 Ma, 5.5 Ma and 2.8 Ma, superimposed on the gradual cooling trend (Fig. 6). Overall, by comparing our mid-latitude SST record with other sites in the southern hemisphere, we show that the latitudinal gradient of the Southern Ocean varied from weak (23–17Ma), to weakened (17–14.5 Ma), to strengthening (14.5–5 Ma), to variable (5–0 Ma) (Fig. 7) which we link to the gradual development of the frontal systems in the Southern Ocean, related to the interplay between ice sheet, tectonic and climatic evolution of the Neogene Southern Ocean. The long-term evolution of subtropical front SSTs is consistent with that of $\delta^{18}O_{bf}$, except for the progressive 10°C cooling in the late Miocene that is less pronounced in $\delta^{18}O_{bf}$

(~0.3 permille) (Fig. 6). Perhaps this reflects a nonlinear response of subtropical front SST to the progressive buildup of ice sheets once it has passed a critical threshold, including that of the west-Antarctic ice sheet (Marschalek et al., 2021), and a more persistent presence of sea ice (Sangiorgi et al., 2018). In general, we observe modest cooling in the equatorial Pacific region throughout the Neogene, and modest cooling also at the Antarctic continental margin. But the strong cooling in the subtropical front region suggests that the shape of the meridional temperature gradient changed fundamentally, with broad warm Southern Ocean in the mid-Miocene and progressive expansion of cold-temperate conditions towards lower latitudes thereafter. This could be caused by a progressive increase in strength of the ACC, strengthening latitudinal SST gradients in mid-to-low latitudes. Further study should reveal the exact changes of both surface oceanographic conditions (not exclusively SST but also upwelling and salinity) and deep-water temperature (including separate deep-water temperature and ice volume signals).

5. Conclusion

Our Neogene SST record from offshore Tasmania, derived from 2 independent biomarker proxies, provides a first continuous, long-term record of subtropical Southern Ocean SST evolution during the gateway opening. The SST record reflects a warm mid-Miocene climatic optimum, a gradual but profound 10°C cooling in the mid-to-late Miocene and renewed warming in the Pliocene and highly variable temperature conditions during the Pleistocene to modern times. The long-term SST trend is consistent with the $\delta^{18}O_{bf}$ record, except during the late Miocene cooling. Short-term SST variability in the record can be linked to glacial-interglacial phases, suggesting strong coupling between Antarctic ice sheet buildup and the subtropical front temperature on a multi-million-year timescale. However, the mechanism of the decoupling between SST and $\delta^{18}O_{bf}$ during the late Miocene is still enigmatic. Comparison with previously published SST records indicates that the latitudinal gradient in the Southern Ocean experienced a stepwise development, from a relatively strong gradient in the early Miocene, to reduced gradients during the MCO, and then steepening during the mid-to-late Miocene. Pliocene to modern time gradients remain relatively constant in trend but may differ in range over glacial-interglacial cycles. During the late Miocene cooling, the latitudinal SST gradient between the STF and Pacific equator profoundly increased (from 4°C to 14°C) while the SST gradient between the STF and the Antarctic margin decreased due to amplified STF cooling and relatively stable near-Antarctic SSTs. This caused a progressive narrowing of the warm equatorial-to-subtropical heat distribution, and an expansion of subpolar conditions to lower latitudes. Our study presents a continuous picture of the STF temperature evolution in the Southern Ocean

Tasmanian gateway area and reveals the history of frontal systems towards modern conditions.

Data availability:

TEX_{86} and $U^{k'}37$ data of ODP Site 1168 is deposited at Zenodo https://doi.org/10.5281/zenodo.7119904.

Competing interests:

The authors declare that they have no conflict of interest

Author contributions:

PKB designed the research. SH, FH and FL processed samples for organic geochemistry (TEX_{86} and $U^{k'}_{37}$). All authors contributed to analysing the data. SH designed the figures and wrote the paper with input from all authors.

Acknowledgements:

We thank Mariska Hoorweg, Klaas Nierop, Desmond Eefting and Addison Rice for laboratory assistance. We thank Johan Weijers, Benjamin Petrick, Guodong Jia, Stefan Schouten, Robert McKay and Bella Duncan for providing corresponding data which were used to interpret the results. We thank IODP and shipboard scientists of ODP 189, especially KCC in Japan for the help with sampling. Additional gratitude is sent to Kun Huang for helping generate Monte-Carlo simulation of GDGTs compositions although not included in the manuscript and Mei Nelissen for preliminary data analysis. This research is funded by ERC Starting Grant 802835 to Peter K. Bijl. We thank the reviewers Igor Obrecht and Benjamin Petrick for their constructive comments that helped improve our manuscript.

References:

Basse, A., Zhu, C., Versteegh, G. J. M., Fischer, G., Hinrichs, K. U., & Mollenhauer, G.: Distribution of intact and core tetraether lipids in water column profiles of suspended particulate matter off Cape Blanc, NW Africa. *Organic Geochemistry*, *72*. https://doi.org/10.1016/j.orggeochem.2014.04.007, 2014.

Besseling, M. A., Hopmans, E. C., Koenen, M., van der Meer, M. T. J., Vreugdenhil, S., Schouten, S., Sinninghe Damsté, J. S., & Villanueva, L.: Depth-related differences in archaeal populations impact the isoprenoid tetraether lipid composition of the Mediterranean Sea water column. *Organic Geochemistry*, *135*. https://doi.org/10.1016/j.orggeochem.2019.06.008, 2019.

Bijl, P.K., Hoem, F.S., & Hou, S.: sea-surface temperature proxy data (TEX86 and UK'37) from Ocean Drilling Program Site 1168 [Data set]. Zenodo. https://doi.org/10.5281/zenodo.7119904, 2022.

Bijl, P. K., Frieling, J., Cramwinckel, M. J., Boschman, C., Sluijs, A., & Peterse, F.: Maastrichtian-Rupelian paleoclimates in the southwest Pacific - A critical re-evaluation of biomarker paleothermometry and dinoflagellate cyst paleoecology at Ocean Drilling Program Site 1172. *Climate of the Past*, *17*(6). https://doi.org/10.5194/cp-17-2393-2021, 2021.

Bijl, P. K., Houben, A. J. P., Hartman, J. D., Pross, J., Salabarnada, A., Escutia, C., & Sangiorgi, F.: Paleoceanography and ice sheet variability offshore Wilkes Land, Antarctica - Part 2: Insights from Oligocene-Miocene dinoflagellate cyst assemblages. *Climate of the Past*, *14*(7), 1015–1033. https://doi.org/10.5194/cp-14-1015-2018, 2018.

Billups, K., Channell, J. E. T., & Zachos, J.: Late Oligocene to early Miocene geochronology and paleoceanography from the subantarctic South Atlantic. *Paleoceanography*, *17*(1). https://doi.org/10.1029/2000pa000568, 2002.

Blaga, C. I., Reichart, G. J., Heiri, O., & Sinninghe Damsté, J. S.: Tetraether membrane lipid distributions in water-column particulate matter and sediments: A study of 47 European lakes along a north-south transect. *Journal of Paleolimnology*, *41*(3), 523–540. https://doi.org/10.1007/s10933-008-9242-2, 2009.

Burls, N. J., Bradshaw, C. D., de Boer, A. M., Herold, N., Huber, M., Pound, M., Donnadieu, Y., Farnsworth, A., Frigola, A., Gasson, E., von der Heydt, A. S., Hutchinson, D. K., Knorr, G., Lawrence, K. T., Lear, C. H., Li, X., Lohmann, G., Lunt, D. J., Marzocchi, A., … Zhang, Z.: Simulating Miocene Warmth: Insights From an Opportunistic Multi-Model Ensemble (MioMIP1). *Paleoceanography and Paleoclimatology*, *36*(5). https://doi.org/10.1029/2020PA004054, 2021.

Chiang, J. C.: The tropics in paleoclimate. *Annual Review of Earth and Planetary Sciences*, *37*, 263-297. DOI: 10.1146/annurev.earth.031208.100217, 2009.

Christensen, B. A., De Vleeschouwer, D., Henderiks, J., Groeneveld, J., Auer, G., Drury, A. J., ... & Kroon, D.: Late Miocene Onset of Tasman Leakage and Southern Hemisphere Supergyre Ushers in Near-Modern Circulation. *Geophysical research letters*, *48*(18), e2021GL095036. https://doi.org/10.1029/2021GL095036, 2021.

Cody, R. D., Levy, R. H., Harwood, D. M., & Sadler, P. M.: Thinking outside the zone: High-resolution quantitative diatom biochronology for the Antarctic Neogene. *Palaeogeography, Palaeoclimatology, Palaeoecology*, *260*(1–2). https://doi.org/10.1016/j.palaeo.2007.08.020, 2008.

Dearing Crampton-Flood, E., Peterse, F., & Sinninghe Damsté, J. S.: Production of branched tetraethers in the marine realm: Svalbard fjord sediments revisited. *Organic Geochemistry*, *138*. https://doi.org/10.1016/j.orggeochem.2019.103907, 2019.

de Boer, A. M., Graham, R. M., Thomas, M. D., & Kohfeld, K. E.: The control of the Southern Hemisphere Westerlies on the position of the subtropical front. *Journal of Geophysical Research: Oceans*, *118*(10). https://doi.org/10.1002/jgrc.20407, 2013.

de Vleeschouwer, D., Petrick, B. F., & Martínez-García, A.: Stepwise Weakening of the Pliocene Leeuwin Current. *Geophysical Research Letters*, *46*(14). https://doi.org/10.1029/2019GL083670, 2019.

Ding, W. H., Yang, H., He, G. Q., & Xie, S.: Effects of oxidative degradation by hydrogen peroxide on tetraethers-based organic proxies. *Q. Sci*, *33*, 39-47. https://doi:10.3969/j.issn.1001-7410.2013.01.05, 2013.

Duncan, B., McKay, R., Levy, R. *et al.* Climatic and tectonic drivers of late Oligocene Antarctic ice volume. *Nat. Geosci*. https://doi.org/10.1038/s41561-022-01025-x, 2022

Eglinton, T. I., & Eglinton, G.: Molecular proxies for paleoclimatology. *Earth and Planetary Science Letters*, *275*(1–2). https://doi.org/10.1016/j.epsl.2008.07.012, 2008.

Evangelinos, D., Escutia, C., van de Flierdt, T., Valero, L., Flores, J. A., Harwood, D. M., Hoem, F. S., Bijl, P., Etourneau, J., Kreissig, K., Nilsson-Kerr, K., Holder, L., López-Quirós, A., & Salabarnada, A.: Absence of a strong, deep-reaching Antarctic Circumpolar Current zonal flow across the Tasmanian gateway during the Oligocene to early Miocene. *Global and Planetary Change*, *208*. https://doi.org/10.1016/j.gloplacha.2021.103718, 2022.

Exon, N. F., Kennett, J. P., Malone, M. J., and the Leg189 Shipboard Scientific Party: Site 1168., Proceedings of the Ocean Drilling Program Initial Reports, Ocean Drilling Program, College Station, TX, USA,, 2001.

Freitas, F. S., Pancost, R. D., & Arndt, S.: The impact of alkenone degradation on U37K′ paleothermometry: A model-derived assessment. *Paleoceanography*, *32*(6). https://doi.org/10.1002/2016PA003043, 2017

Gaskell, D. E., Huber, M., O'Brien, C. L., Inglis, G. N., Acosta, R. P., Poulsen, C. J., & Hull, P. M.: The latitudinal temperature gradient and its climate dependence as inferred from foraminiferal δ18O over the past 95 million years. *Proceedings of the National Academy of Sciences of the United States of America*, *119*(11). https://doi.org/10.1073/pnas.2111332119, 2022.

Gradstein, F. M., & Ogg, J. G.: The Chronostratigraphic Scale. In *Geologic Time Scale 2020*. https://doi.org/10.1016/B978-0-12-824360-2.00002-4, 2020.

Gourley, T. L., & Gallagher, S. J.: Foraminiferal biofacies of the Miocene warm to cool climatic transition in the Port Phillip Basin, southeastern Australia. *The Journal of Foraminiferal Research,* 34(4), 294-307, https://doi.org/10.2113/34.4.294, 2004.

Groeneveld, J., Henderiks, J., Renema, W., McHugh, C. M., de Vleeschouwer, D., Christensen, B. A., Fulthorpe, C. S., Reuning, L., Gallagher, S. J., Bogus, K., Auer, G., & Ishiwa, T.: Australian shelf sediments reveal shifts in Miocene Southern Hemisphere westerlies. *Science Advances*, *3*(5). https://doi.org/10.1126/sciadv.1602567, 2017.

Guitián, J., & Stoll, H. M.: Evolution of Sea Surface Temperature in the Southern Mid-latitudes From Late Oligocene Through Early Miocene. *Paleoceanography and Paleoclimatology*, *36*(9). https://doi.org/10.1029/2020PA004199, 2021.

Hartman, J. D., Sangiorgi, F., Salabarnada, A., Peterse, F., Houben, A. J. P., Schouten, S., Brinkhuis, H., Escutia, C., & Bijl, P. K.: Paleoceanography and ice sheet variability offshore Wilkes Land, Antarctica-Part 3: Insights from Oligocene-Miocene TEX86-based sea surface temperature reconstructions. *Climate of the Past*, *14*(9), 1275–1297. https://doi.org/10.5194/cp-14-1275-2018, 2018.

He, Y., Wang, H., & Liu, Z.: Development of the Leeuwin Current on the northwest shelf of Australia through the Pliocene-Pleistocene period. *Earth and Planetary Science Letters*, *559*. https://doi.org/10.1016/j.epsl.2021.116767, 2021.

Heath, R. A.: A review of the physical oceanography of the seas around New Zealand — 1982. *New Zealand Journal of Marine and Freshwater Research*, *19*(1). https://doi.org/10.1080/00288330.1985.9516077, 1985.

Herbert, T. D., Lawrence, K. T., Tzanova, A., Peterson, L. C., Caballero-Gill, R., & Kelly, C. S.: Late Miocene global cooling and the rise of modern ecosystems. *Nature Geoscience*, *9*(11), 843–847. https://doi.org/10.1038/ngeo2813, 2016.

Hernández-Sánchez, M. T., Woodward, E. M. S., Taylor, K. W. R., Henderson, G. M., & Pancost, R. D.: Variations in GDGT distributions through the water column in the South East Atlantic Ocean. *Geochimica et Cosmochimica Acta*, *132*, 337–348. https://doi.org/10.1016/j.gca.2014.02.009, 2014.

Herold, N., Huber, M., Müller, R. D., & Seton, M.: Modeling the Miocene climatic optimum: Ocean circulation. *Paleoceanography*, *27*(1). https://doi.org/10.1029/2010PA002041, 2012.

Herold, N., Huber, M., & Müller, R. D.: Modeling the miocene climatic optimum. Part I: Land and atmosphere. *Journal of Climate*, *24*(24). https://doi.org/10.1175/2011JCLI4035.1, 2011.

Hoem, F. S., Sauermilch, I., Hou, S., Brinkhuis, H., Sangiorgi, F., & Bijl, P. K.: Late Eocene-early Miocene evolution of the southern Australian subtropical front: a marine palynological approach. *Journal of Micropalaeontology*, *40*(2). https://doi.org/10.5194/jm-40-175-2021, 2021.

Hoem, F. S., Sauermilch, I., Aleksinski, A. K., Huber, M., Peterse, F., Sangiorgi, F., & Bijl, P. K.: Strength and variability of the Oligocene Southern Ocean surface temperature gradient. *Communications Earth & Environment*, 3(1), 1-8. https://doi.org/10.1038/s43247-022-00666-5, 2022.

Ho, S. L., & Laepple, T.: Flat meridional temperature gradient in the early Eocene in the subsurface rather than surface ocean. *Nature Geoscience*, *9*(8), 606–610. https://doi.org/10.1038/ngeo2763, 2016.

Holbourn, A., Kuhnt, W., Clemens, S., Prell, W., & Andersen, N.: Middle to late Miocene stepwise climate cooling: Evidence from a high-resolution deep water isotope curve spanning 8 million years. *Paleoceanography*, *28*(4). https://doi.org/10.1002/2013PA002538, 2013.

Hopmans, E. C., Schouten, S., & Sinninghe Damsté, J. S.: The effect of improved chromatography on GDGT-based palaeoproxies. *Organic Geochemistry*, *93*. https://doi.org/10.1016/j.orggeochem.2015.12.006, 2016.

Hopmans, E. C., Weijers, J. W. H., Schefuß, E., Herfort, L., Sinninghe Damsté, J. S., & Schouten, S.: A novel proxy for terrestrial organic matter in sediments based on branched and isoprenoid tetraether lipids. *Earth and Planetary Science Letters*,

224(1–2), 107–116. https://doi.org/10.1016/j.epsl.2004.05.012, 2004.

Huguet, C., de Lange, G. J., Gustafsson, Ö., Middelburg, J. J., Sinninghe Damsté, J. S., & Schouten, S.: Selective preservation of soil organic matter in oxidized marine sediments (Madeira Abyssal Plain). *Geochimica et Cosmochimica Acta*, *72*(24). https://doi.org/10.1016/j.gca.2008.09.021, 2008.

Hurley, S. J., Lipp, J. S., Close, H. G., Hinrichs, K. U., & Pearson, A.: Distribution and export of isoprenoid tetraether lipids in suspended particulate matter from the water column of the Western Atlantic Ocean. *Organic Geochemistry*, *116*. https://doi.org/10.1016/j.orggeochem.2017.11.010, 2018.

Jackson, C. A. L., Magee, C., & Hunt-Stewart, E. R.: Cenozoic contourites in the eastern great australian bight, offshore southern Australia: Implications for the onset of the Leeuwin Current. *Journal of Sedimentary Research*, *89*(3). https://doi.org/10.2110/jsr.2019.16, 2019.

Kim, J. H., van der Meer, J., Schouten, S., Helmke, P., Willmott, V., Sangiorgi, F., Koç, N., Hopmans, E. C., & Damsté, J. S. S. New indices and calibrations derived from the distribution of crenarchaeal isoprenoid tetraether lipids: Implications for past sea surface temperature reconstructions. *Geochimica et Cosmochimica Acta*, *74*(16), 4639–4654. https://doi.org/10.1016/j.gca.2010.05.027, 2010.

Kim, J. H., Schouten, S., Rodrigo-Gámiz, M., Rampen, S., Marino, G., Huguet, C., Helmke, P., Buscail, R., Hopmans, E. C., Pross, J., Sangiorgi, F., Middelburg, J. B. M., & Sinninghe Damsté, J. S. Influence of deep-water derived isoprenoid tetraether lipids on the TEX86H paleothermometer in the Mediterranean Sea. *Geochimica et Cosmochimica Acta*, *150*. https://doi.org/10.1016/j.gca.2014.11.017, 2015.

Kim, J. H., Villanueva, L., Zell, C., & Sinninghe Damsté, J. S.: Biological source and provenance of deep-water derived isoprenoid tetraether lipids along the Portuguese continental margin. *Geochimica et Cosmochimica Acta*, *172*. https://doi.org/10.1016/j.gca.2015.09.010, 2016.

Kim, B., & Zhang, Y. G.: Methane hydrate dissociation across the Oligocene–Miocene boundary. *Nature Geoscience*, *15*(3). https://doi.org/10.1038/s41561-022-00895-5, 2022.

Lear, C. H., Coxall, H. K., Foster, G. L., Lunt, D. J., Mawbey, E. M., Rosenthal, Y., Sosdian, S. M., Thomas, E., & Wilson, P. A.: Neogene ice volume and ocean temperatures: Insights from infaunal foraminiferal Mg/Ca paleothermometry. *Paleoceanography*, *30*(11). https://doi.org/10.1002/2015PA002833, 2015.

Leutert, T. J., Modestou, S., Bernasconi, S. M., & Meckler, A. N.: Southern ocean bottom-water cooling and ice sheet expansion during the middle Miocene climate transition. *Climate of the Past*, *17*(5). https://doi.org/10.5194/cp-17-2255-2021, 2021.

Leutert, T. J., Auderset, A., Martínez-García, A., Modestou, S., & Meckler, A. N.: Coupled Southern Ocean cooling and Antarctic ice sheet expansion during the middle Miocene. *Nature Geoscience*, *13*(9). https://doi.org/10.1038/s41561-020-0623-0, 2020.

Levy, R., Harwood, D., Florindo, F., Sangiorgi, F., Tripati, R., von Eynatten, H., Gasson, E., Kuhn, G., Tripati, A., Deconto,

R., Fielding, C., Field, B., Golledge, N., McKay, R., Naish, T., Olney, M., Pollard, D., Schouten, S., Talarico, F., … Zattin, M.: Antarctic ice sheet sensitivity to atmospheric CO 2 variations in the early to mid-Miocene. *Proceedings of the National Academy of Sciences of the United States of America*, *113*(13). https://doi.org/10.1073/pnas.1516030113, 2016.

Lewis, A. R., Marchant, D. R., Ashworth, A. C., Hemming, S. R., & Machlus, M. L.: Major middle Miocene global climate change: Evidence from East Antarctica and the Transantarctic Mountains. *Geological Society of America Bulletin*, *119*(11). https://doi.org/10.1130/b26134, 2007.

Liebrand, D., Lourens, L. J., Hodell, D. A., de Boer, B., van de Wal, R. S. W., & Pälike, H.: Antarctic ice sheet and oceanographic response to eccentricity forcing during the early Miocene. *Climate of the Past*, *7*(3). https://doi.org/10.5194/cp-7-869-2011, 2011.

Marschalek, J. W., Zurli, L., Talarico, F., van de Flierdt, T., Vermeesch, P., Carter, A., Beny, F., Bout-Roumazeilles, V., Sangiorgi, F., Hemming, S. R., Pérez, L. F., Colleoni, F., Prebble, J. G., van Peer, T. E., Perotti, M., Shevenell, A. E., Browne, I., Kulhanek, D. K., Levy, R., … Xiong, Z.: A large West Antarctic Ice Sheet explains early Neogene sea-level amplitude. *Nature*, *600*(7889). https://doi.org/10.1038/s41586-021-04148-0, 2021.

McGowran, B., Holdgate, G. R., Li, Q., & Gallagher, S. J.: Cenozoic stratigraphic succession in southeastern Australia. *Australian Journal of Earth Sciences*, *51*(4). https://doi.org/10.1111/j.1400-0952.2004.01078.x, 2004.

McGowran, B., Qianyu, L., Cann, J., Padley, D., McKirdy, D. M., & Shafik, S.: Biogeographic impact of the Leeuwin Current in southern Australia since the late middle Eocene. *Palaeogeography, Palaeoclimatology, Palaeoecology*, *136*(1–4). https://doi.org/10.1016/S0031-0182(97)00073-4, 1997.

McKay, R., Naish, T., Carter, L., Riesselman, C., Dunbar, R., Sjunneskog, C., Winter, D., Sangiorgi, F., Warren, C., Pagani, M., Schouten, S., Willmott, V., Levy, R., DeConto, R., & Powell, R. D.: Antarctic and Southern Ocean influences on Late Pliocene global cooling. *Proceedings of the National Academy of Sciences of the United States of America*, *109*(17). https://doi.org/10.1073/pnas.1112248109, 2012.

Meckler, A. N., Sexton, P. F., Piasecki, A. M., Leutert, T. J., Marquardt, J., Ziegler, M., ... & Bernasconi, S. M. Cenozoic evolution of deep ocean temperature from clumped isotope thermometry. *Science*, *377*(6601), 86-90. https://doi.org/10.1126/science.abk0604, 2022

Miller, K. G., Wright, J. D., & Fairbanks, R. G.: Unlocking the ice house: Oligocene-Miocene oxygen isotopes, eustasy, and margin erosion. *Journal of Geophysical Research*, *96*(B4). https://doi.org/10.1029/90JB02015, 1991.

Modestou, S. E., Leutert, T. J., Fernandez, A., Lear, C. H., & Meckler, A. N.: Warm Middle Miocene Indian Ocean Bottom Water Temperatures: Comparison of Clumped Isotope and Mg/Ca-Based Estimates. *Paleoceanography and Paleoclimatology*, *35*(11). https://doi.org/10.1029/2020PA003927, 2020.

Passchier, S., Browne, G., Field, B., Fielding, C. R., Krissek, L. A., Panter, K., & Pekar, S. F.: Early and middle miocene antarctic glacial history from the sedimentary facies distribution in the AND-2A drill hole, Ross sea, Antarctica. *Bulletin of the*

Geological Society of America, *123*(11–12). https://doi.org/10.1130/B30334.1, 2011.

Peterse, F., Kim, J. H., Schouten, S., Kristensen, D. K., Koç, N., & Sinninghe Damsté, J. S.: Constraints on the application of the MBT/CBT palaeothermometer at high latitude environments (Svalbard, Norway). *Organic Geochemistry*, *40*(6). https://doi.org/10.1016/j.orggeochem.2009.03.004, 2009.

Pfuhl, H. A., McCave, I. N., Schellenberg, S. A., & Ferretti, P.: Changes in southern ocean circulation in late oligocene to early miocene time. In *Geophysical Monograph Series* (Vol. 151). https://doi.org/10.1029/151GM11, 2004.

Prahl, F. G., & Wakeham, S. G.: Calibration of unsaturation patterns in long-chain ketone compositions for palaeotemperature assessment. *Nature*, *330*(6146). https://doi.org/10.1038/330367a0, 1987.

Rae, J. W. B., Zhang, Y. G., Liu, X., Foster, G. L., Stoll, H. M., & Whiteford, R. D. M.: Atmospheric cobinf2einf over the past 66 million years from marine archives. In *Annual Review of Earth and Planetary Sciences* (Vol. 49). https://doi.org/10.1146/annurev-earth-082420-063026, 2021.

Ransom, B., Kim, D., Kastner, M., & Wainwright, S.: Organic matter preservation on continental slopes: importance of mineralogy and surface area. *Geochimica et Cosmochimica Acta*, *62*(8). https://doi.org/10.1016/S0016-7037(98)00050-7, 1998.

Rintoul, S. R., Chown, S. L., DeConto, R. M., England, M. H., Fricker, H. A., Masson-Delmotte, V., Naish, T. R., Siegert, M. J., & Xavier, J. C.: Choosing the future of Antarctica. In *Nature* (Vol. 558, Issue 7709). https://doi.org/10.1038/s41586-018-0173-4, 2018.

Robert, C.: Data Report: Bulk and Clay Mineral Assemblages of the Tasmanian Area, Maastrichtian–Pleistocene, ODP Leg 189. In *Proceedings of the Ocean Drilling Program, 189 Scientific Results*. https://doi.org/10.2973/odp.proc.sr.189.114.2004, 2004.

Rousselle, G., Beltran, C., Sicre, M. A., Raffi, I., & de Rafélis, M.: Changes in sea-surface conditions in the Equatorial Pacific during the middle Miocene-Pliocene as inferred from coccolith geochemistry. *Earth and Planetary Science Letters*, *361*. https://doi.org/10.1016/j.epsl.2012.11.003, 2013.

Rosell-Melé, A., Carter, J., & Eglinton, G.: Distributions of long-chain alkenones and alkyl alkenoates in marine surface sediments from the North East Atlantic. *Organic Geochemistry*, *22*(3-5), 501-509., https://doi.org/10.1016/0146-6380(94)90122-8, 1994.

Sangiorgi, F., Bijl, P. K., Passchier, S., Salzmann, U., Schouten, S., McKay, R., Cody, R. D., Pross, J., van de Flierdt, T., Bohaty, S. M., Levy, R., Williams, T., Escutia, C., & Brinkhuis, H.: Southern Ocean warming and Wilkes Land ice sheet retreat during the mid-Miocene. *Nature Communications*, *9*(1), 1–11. https://doi.org/10.1038/s41467-017-02609-7, 2018.

Sangiorgi, Francesca: Miocene ocean temperatures (TEX86-L) of the ANDRILL-2A record, Ross Sea, Antarctica. PANGAEA, https://doi.org/10.1594/PANGAEA.914002, 2020

Sauermilch, I., Whittaker, J. M., Klocker, A., Munday, D. R., Hochmuth, K., Bijl, P. K., & LaCasce, J. H.: Gateway-driven

设置了格式：字体：（默认）Times New Roman

设置了格式：字体：（默认）Times New Roman

设置了格式：字体：（默认）Times New Roman，10 磅，下划线，字体颜色：蓝色

域代码已更改

设置了格式：字体：（默认）Times New Roman，10 磅

weakening of ocean gyres leads to Southern Ocean cooling. *Nature Communications*, *12*(1). https://doi.org/10.1038/s41467-021-26658-1, 2021.

Scher, H. D., Whittaker, J. M., Williams, S. E., Latimer, J. C., Kordesch, W. E. C., & Delaney, M. L.: Onset of Antarctic Circumpolar Current 30 million years ago as Tasmanian Gateway aligned with westerlies. *Nature*, *523*(7562). https://doi.org/10.1038/nature14598, 2015.

Schouten, S., Hopmans, E. C., Schefuß, E., & Sinninghe Damsté, J. S.: Distributional variations in marine crenarchaeotal membrane lipids: A new tool for reconstructing ancient sea water temperatures? *Earth and Planetary Science Letters*, *204*(1–2). https://doi.org/10.1016/S0012-821X(02)00979-2, 2002.

Schouten, S., Hopmans, E. C., & Sinninghe Damsté, J. S.: The organic geochemistry of glycerol dialkyl glycerol tetraether lipids: A review. In *Organic Geochemistry* (Vol. 54). https://doi.org/10.1016/j.orggeochem.2012.09.006, 2013.

Shevenell, A. E., Kennett, J. P., & Lea, D. W.: Middle Miocene ice sheet dynamics, deep-sea temperatures, and carbon cycling: A Southern Ocean perspective. *Geochemistry, Geophysics, Geosystems*, *9*(2). https://doi.org/10.1029/2007GC001736, 2008.

Shevenell, A. E., Kennett, J. P., & Lea, D. W.: Middle Miocene Southern Ocean cooling and antarctic cryosphere expansion. *Science*, *305*(5691). https://doi.org/10.1126/science.1100061, 2004.

Sijp, W. P., von der Heydt, A. S., Dijkstra, H. A., Flögel, S., Douglas, P. M. J., & Bijl, P. K.: The role of ocean gateways on cooling climate on long time scales. *Global and Planetary Change*, *119*, 1–22. https://doi.org/10.1016/j.gloplacha.2014.04.004, 2014.

Sinninghe Damsté, J. S.: Spatial heterogeneity of sources of branched tetraethers in shelf systems: The geochemistry of tetraethers in the Berau River delta (Kalimantan, Indonesia). *Geochimica et Cosmochimica Acta*, *186*. https://doi.org/10.1016/j.gca.2016.04.033, 2016.

Skinner, L. C., Fallon, S., Waelbroeck, C., Michel, E., & Barker, S.: Ventilation of the deep southern ocean and deglacial CO2 rise. *Science*, *328*(5982). https://doi.org/10.1126/science.1183627, 2010.

Sluijs, A., Frieling, J., N. Inglis, G., Nierop, K. G. J., Peterse, F., Sangiorgi, F., & Schouten, S.: Late Paleocene-early Eocene Arctic Ocean sea surface temperatures: Reassessing biomarker paleothermometry at Lomonosov Ridge. *Climate of the Past*, *16*(6). https://doi.org/10.5194/cp-16-2381-2020, 2020.

Sosdian, S. M., Greenop, R., Hain, M. P., Foster, G. L., Pearson, P. N., & Lear, C. H.: Constraining the evolution of Neogene ocean carbonate chemistry using the boron isotope pH proxy. *Earth and Planetary Science Letters*, *498*. https://doi.org/10.1016/j.epsl.2018.06.017, 2018.

Stickley, C. E., Brinkhuis, H., McGonigal, K. L., Chaproniere, G. C. H., Fuller, M., Kelly, D. C., Nürnberg, D., Pfuhl, H. A., Schellenberg, S. A., Schoenfeld, J., Suzuki, N., Touchard, Y., Wei, W., Williams, G. L., Lara, J., & Stant, S. A.: Late Cretaceous–Quaternary Biomagnetostratigraphy of ODP Sites 1168, 1170, 1171, and 1172, Tasmanian Gateway. In *Proceedings of the Ocean Drilling Program, 189 Scientific Results*. https://doi.org/10.2973/odp.proc.sr.189.111.2004, 2004.

Super, J. R., Thomas, E., Pagani, M., Huber, M., O'Brien, C. L., & Hull, P. M.: Miocene Evolution of North Atlantic Sea Surface Temperature. *Paleoceanography and Paleoclimatology*, *35*(5), 1–15. https://doi.org/10.1029/2019PA003748, 2020.

Super, J. R., Thomas, E., Pagani, M., Huber, M., O'Brien, C., & Hull, P. M. North Atlantic temperature and pCO2 coupling in the early-middle Miocene. *Geology*, *46*(6), 519–522. https://doi.org/10.1130/G40228.1, 2018.

Tanner, T., Hernández-Almeida, I., Drury, A. J., Guitián, J., & Stoll, H.: Decreasing Atmospheric CO2 During the Late Miocene Cooling. *Paleoceanography and Paleoclimatology*, *35*(12). https://doi.org/10.1029/2020PA003925, 2020.

Tierney, J. E., & Tingley, M. P.: BAYSPLINE: A New Calibration for the Alkenone Paleothermometer. *Paleoceanography and Paleoclimatology*, *33*(3). https://doi.org/10.1002/2017PA003201, 2018.

Tierney, J. E., & Tingley, M. P.: A TEX86 surface sediment database and extended Bayesian calibration. *Sci Data* 2, 150029., https://doi.org/10.1038/sdata.2015.29, 2015.

Tierney, J. E., & Tingley, M. P.: A Bayesian, spatially-varying calibration model for the TEX86 proxy. *Geochimica et Cosmochimica Acta*, *127*, 83–106. https://doi.org/10.1016/j.gca.2013.11.026, 2014.

Taylor, K. W. R., Huber, M., Hollis, C. J., Hernandez-Sanchez, M. T., & Pancost, R. D.: Re-evaluating modern and Palaeogene GDGT distributions: Implications for SST reconstructions. *Global and Planetary Change*, *108*, 158–174. https://doi.org/10.1016/j.gloplacha.2013.06.011, 2013.

Toggweiler, J. R., Russell, J. L., & Carson, S. R.: Midlatitude westerlies, atmospheric CO2, and climate change during the ice ages. *Paleoceanography*, *21*(2). https://doi.org/10.1029/2005PA001154, 2006.

Torsvik, T. H., van der Voo, R., Preeden, U., mac Niocaill, C., Steinberger, B., Doubrovine, P. v., van Hinsbergen, D. J. J., Domeier, M., Gaina, C., Tohver, E., Meert, J. G., McCausland, P. J. A., & Cocks, L. R. M.: Phanerozoic Polar Wander, Palaeogeography and Dynamics. In *Earth-Science Reviews* (Vol. 114, Issues 3–4). https://doi.org/10.1016/j.earscirev.2012.06.007, 2012.

van der Weijst, C. M. H., van der Laan, K. J., Peterse, F., Reichart, G.-J., Sangiorgi, F., Schouten, S., Veenstra, T. J. T., and Sluijs, A.: A 15-million-year surface- and subsurface-integrated TEX_{86} temperature record from the eastern equatorial Atlantic, Clim. Past, 18, 1947–1962, https://doi.org/10.5194/cp-18-1947-2022, 2022.

van Hinsbergen, D. J. J., de Groot, L. v., van Schaik, S. J., Spakman, W., Bijl, P. K., Sluijs, A., Langereis, C. G., & Brinkhuis, H.: A paleolatitude calculator for paleoclimate studies. *PLoS ONE*, *10*(6). https://doi.org/10.1371/journal.pone.0126946, 2015.

Volkman, J. K., Eglinton, G., Corner, E. D. S., & Forsberg, T. E. V.: Long-chain alkenes and alkenones in the marine coccolithophorid Emiliania huxleyi. *Phytochemistry*, *19*(12). https://doi.org/10.1016/S0031-9422(00)83930-8, 1980.

Wakeham, S. G., Lewis, C. M., Hopmans, E. C., Schouten, S., & Sinninghe Damsté, J. S.: Archaea mediate anaerobic oxidation of methane in deep euxinic waters of the Black Sea. *Geochimica et Cosmochimica Acta*, *67*(7). https://doi.org/10.1016/S0016-7037(02)01220-6, 2003.

Weijers, J. W. H., Lim, K. L. H., Aquilina, A., Damsté, J. S. S., & Pancost, R. D.: Biogeochemical controls on glycerol dialkyl

glycerol tetraether lipid distributions in sediments characterized by diffusive methane flux. *Geochemistry, Geophysics, Geosystems*, *12*(10), 1–15. https://doi.org/10.1029/2011GC003724, 2011.

Weijers, J. W. H., Schouten, S., Spaargaren, O. C., & Sinninghe Damsté, J. S.: Occurrence and distribution of tetraether membrane lipids in soils: Implications for the use of the TEX86 proxy and the BIT index. *Organic Geochemistry*, *37*(12). https://doi.org/10.1016/j.orggeochem.2006.07.018, 2006.

Westerhold, T., Marwan, N., Drury, A. J., Liebrand, D., Agnini, C., Anagnostou, E., Barnet, J. S. K., Bohaty, S. M., de Vleeschouwer, D., Florindo, F., Frederichs, T., Hodell, D. A., Holbourn, A. E., Kroon, D., Lauretano, V., Littler, K., Lourens, L. J., Lyle, M., Pälike, H., … Zachos, J. C.: An astronomically dated record of Earth's climate and its predictability over the last 66 million years. *Science*, *369*(6509). https://doi.org/10.1126/SCIENCE.ABA6853, 2020.

Wu, W., Xu, Y., Hou, S., Dong, L., Liu, H., Wang, H., Liu, W., & Zhang, C.: Origin and preservation of archaeal intact polar tetraether lipids in deeply buried sediments from the South China Sea. *Deep-Sea Research Part I: Oceanographic Research Papers*, *152*. https://doi.org/10.1016/j.dsr.2019.103107, 2019.

Zhang, Y. G., Zhang, C. L., Liu, X. L., Li, L., Hinrichs, K. U., & Noakes, J. E.: Methane Index: A tetraether archaeal lipid biomarker indicator for detecting the instability of marine gas hydrates. *Earth and Planetary Science Letters*, *307*(3–4), 525–534. https://doi.org/10.1016/j.epsl.2011.05.031, 2011.

Zhang, Y. G., Pagani, M., & Liu, Z.: A 12-million-year temperature history of the tropical pacific ocean. *Science*, *344*(6179). https://doi.org/10.1126/science.1246172, 2014.

Zhang, Y. G., Pagani, M., & Wang, Z.: Ring Index: A new strategy to evaluate the integrity of TEX86 paleothermometry. *Paleoceanography*, *31*(2), 220–232. https://doi.org/10.1002/2015PA002848, 2016.

Zhang, L., Hay, W. W., Wang, C., & Gu, X.: The evolution of latitudinal temperature gradients from the latest Cretaceous through the Present. In *Earth-Science Reviews* (Vol. 189). https://doi.org/10.1016/j.earscirev.2019.01.025, 2019.

Zheng, Y., Heng, P., Conte, M. H., Vachula, R. S., & Huang, Y.: Systematic chemotaxonomic profiling and novel paleotemperature indices based on alkenones and alkenoates: Potential for disentangling mixed species input. *Organic Geochemistry*, 128, 26–41. https://doi.org/10.1016/j.orggeochem.2018.12.008, 2019